Hydrothermal Fabrication of High Specific Surface Area Mesoporous MgO with Excellent CO_2 Adsorption Potential at Intermediate Temperatures

Wanlin Gao [1], Tuantuan Zhou [1], Benoit Louis [2] and Qiang Wang [1],*

[1] College of Environmental Science and Engineering, Beijing Forestry University, 35 Qinghua East Road, Haidian District, Beijing 100083, China; gaowanlin2016@bjfu.edu.cn (W.G.); ztuant86@126.com (T.Z.)

[2] Laboratoire de Synthèse, Réactivité Organiques et Catalyse, Institut de Chimie, UMR 7177, Université de Strasbourg, 1 rue Blaise Pascal, 67000 Strasbourg, France; blouis@unistra.fr

* Correspondence: qiangwang@bjfu.edu.cn; Tel.: +86-136-9913-0626

Abstract: In this work, we report on a novel sodium dodecyl sulfate (SDS)-assisted magnesium oxide (MgO)-based porous adsorbent synthesized by hydrothermal method for intermediate CO_2 capture. For industrial MgO, its CO_2 adsorption capacity is normally less than 0.06 mmol g^{-1}, with a specific surface area as low as 25.1 m^2 g^{-1}. Herein, leaf-like MgO nanosheets which exhibited a disordered layer structure were fabricated by the introduction of SDS surfactants and the control of other synthesis parameters. This leaf-like MgO adsorbent showed an excellent CO_2 capacity of 0.96 mmol g^{-1} at moderate temperatures (~300 °C), which is more than ten times higher than that of the commercial light MgO. This novel mesoporous MgO adsorbent also exhibited high stability during multiple CO_2 adsorption/desorption cycles. The excellent CO_2 capturing performance was believed to be related to its high specific surface area of 321.3 m^2 g^{-1} and abundant surface active adsorption sites. This work suggested a new synthesis scheme for MgO based CO_2 adsorbents at intermediate temperatures, providing a competitive candidate for capturing CO_2 from certain sorption enhanced hydrogen production processes.

Keywords: sorption enhanced water gas shift reaction; CO_2 adsorption; magnesium oxides; hydrothermal synthesis; SDS

1. Introduction

The increased atmospheric CO_2 concentration and the resulting global warming and anthropogenic climate change are the price we pay for over-industrialized developments and excessive combustion of fossil fuels [1–3]. It is well accepted that the CO_2 released by persistent combustion of fossil fuel is one of the main reasons for the average global temperature increase and disastrous environmental effects [4–6]. It is estimated that fossil fuels will still be the dominant supply to meet the energy demand of the future. Such a trend will make it impossible for us to halt the increase in atmospheric CO_2 levels immediately [7,8]. Recently, the introduction of CO_2 capture, storage (sequestration), and utilization (CSU) systems has received substantial attention because of their potential for restricting the release of anthropogenic CO_2 and improving the energy utilization efficiency. Behind the technologies, suitable CO_2 capturing materials are crucial for the establishment of the advanced CSU systems [5,9,10].

So was born three main approaches or processes to capture CO_2 from point sources, that is pre-combustion capture, post-combustion capture and oxyfuel combustion [11]. Among these, solid adsorbents have been commonly fit for the integrated gasification combined cycles (IGCC) related

pre-combustion CO_2 capture processes [4,5], e.g., sorption enhanced water gas shift (SEWGS) and sorption enhanced biomass reforming (SEBR) reactions [12–15]. Among the abundant solid adsorbents which tend to capture CO_2 at moderate temperatures [5,14–16], layered double hydroxides (LDHs) derived metal oxides [17–21] and magnesium oxide (MgO) based compounds [22–26] are promising for the SEWGS and SEBR technologies in the temperature range of 200-400 °C [10,27–30]. LDHs have the reputation of outstanding thermal stability and relatively fast CO_2 adsorption kinetics. They also have the advantage of being regenerated at an intermediate temperature [31–33]. Furthermore, MgO materials have been attracting intense attention as a suitable adsorbent for effective capture of CO_2 as much progress has been obtained within a short period of time [4,15,34,35]. Two factors weigh heavily against the effectiveness of pure MgO in CO_2 capture performance. One is the poor thermal stability during regeneration, and the other is the lack of enough surface basic sites due to a low specific surface area (less than 25.1 m^2 g^{-1}) [23,36–38].

Due to the drawbacks of commercial MgO adsorbent, researchers adopted various methods for the fabrication of porous MgO materials with a large specific surface area [39]. Herein, we report a facile fabrication of pretty high specific surface area (>321.3 m^2 g^{-1}) mesoporous MgO by a urea hydrolysis process from magnesium nitrate aqueous solution followed by thermal decomposition of the precipitated precursors. The synthesized material has also been compared for CO_2 capture capacity and kinetics with the commercial light MgO and the MgO samples obtained from thermal decomposition of commercial magnesium hydroxide. The influences of surfactant species, the ratio of ethanol and water, surfactant loading, calcination temperature, reaction time, and reaction temperature were investigated systematically to attain the maximum CO_2 capture capacity of the compounds. Typically, the sodium dodecyl sulfate (SDS)-assisted MgO materials possessed the highest CO_2 capture capacity of 0.96 mmol g^{-1} at moderate temperatures (~300 °C). The cycling performance of this SDS-assisted porous MgO as a CO_2 adsorbent was evaluated under multiple cycles by thermogravimetric analysis (TGA) using temperature swing adsorption (TSA) with different CO_2 concentrations. Finally, the optimized SDS-assisted MgO adsorbent was characterized in depth.

2. Results and Discussion

### 2.1. Evaluation of CO$_2$ Adsorption Capacity

To clarify the key factors determining the performance of the MgO materials, the influences of different types of surfactants, ratio of ethanol and water, SDS amount, reaction time, and reaction temperature were systematically studied using X-ray diffractometry (XRD), scanning electron microscopy (SEM), Fourier transform infrared spectroscopy (FTIR), thermogravimetric analyzer (TGA) and Brunauer-Emmett-Teller (BET) analyses, as presented in detail in the following sections.

2.1.1. The Influence of Different Types of Surfactant on CO_2 Capture

With the introduction of surfactants as templates, the synthesized MgO nanomaterials exhibited a specific morphology and a high specific surface area. In order to evaluate the effect of the surfactant types, different MgO samples were synthesized using a variety of surfactants, including poly (ethylene glycol)-poly (propylene glycol)-poly(ethylene glycol) triblock copolymer (P-123), polyvinylpyrrolidone (PVP), cetyl trimethyl ammonium bromide (CTAB), and sodium dodecyl sulfate (SDS). Meanwhile, the CO_2 adsorption capacity of non-assisted MgO, MgO attained through thermal decomposition of commercial $Mg(OH)_2$ (coded as MgO-TD) as well as light MgO were studied simultaneously and compared as the control. Table 1 summarizes the synthetic conditions, texture parameters, and CO_2 adsorption capacities of different types of surfactant-assisted MgO. The adoption of a hydrothermal synthesis method with the introduction of various surfactants led to a marked enhancement in the CO_2 uptake of the MgO materials. Except for the sample of light MgO, all other freshly prepared MgO compounds showed a much higher BET specific surface area (>194.3 m^2 g^{-1}) and a larger pore volume (>0.30 cm^{-3} g^{-1}). The addition of surfactants gave rise to a significant increase in specific

surface area from 194.3 to 341.4 $m^2\ g^{-1}$ and pore volume from 0.30 to 0.49 $cm^{-3}\ g^{-1}$, respectively. Figure 1a shows the uptake of CO_2 by non-assisted MgO, MgO-TD, light MgO and MgO particles assisted with various surfactants when exposed at 300 °C to pure CO_2. Typically, the light-MgO was first calcined at 450 °C for 60 min under a flow of high purity N_2 (20 mL min^{-1}) to avoid intrinsic adsorption of CO_2 on the surface of light-MgO. It is clear that SDS-assisted MgO exhibited the highest CO_2 uptake of 0.92 mmol g^{-1}, which is much higher than that of light MgO (0.05 mmol g^{-1}). For the SDS-added sample, although its CO_2 adsorption capacity per unit surface area (0.0028 mmol m^{-2}) was lower than that for the surfactant-free sample (0.0044 mmol m^{-2}), its specific surface area was higher, thus resulting in a much higher total CO_2 capture capacity. For the practical application, the total CO_2 capture capacity is more important. Besides, the MgO-TD with the highest specific surface area of 363.40 $m^2\ g^{-1}$ yet displayed inferior CO_2 uptake of 0.29 mmol g^{-1}. The intrinsic reason for such phenomenon is still unclear to us. Although, the specific surface area and pore size are believed to be two of the parameters that influence the CO_2 capture capacity, some other parameters including chemical impurity, surface defects, etc. may have quite an influence [40].

The XRD patterns of all samples are also provided for better explanation, as shown in Figure 1b. The characteristic peaks of MgO (JCPDS 45-0946) at 2θ = 42.89° and 62.41° are clearly observed, revealing the formation of well-crystallized MgO. Table 1 summarizes the average size of crystalline domains calculated from XRD patterns according to Scherrer formula. Surfactant-assisted samples have the average crystallite sizes of less than 8 nm, much smaller than that of light MgO (32.4 nm) for the in templating with various surfactants. The introduction of surfactant appears to be beneficial for the formation of small MgO nanocrystal structure. Among all the samples, CTAB and SDS showed almost identical CO_2 uptake. Although it seemed that CTAB yielded better textural properties in terms of specific surface area and pore volume, no much difference was observed with the SDS assisted one. In this work, our aim is to optimize the CO_2 capture capacity of surfactant-assisted MgO materials to a great extent while SDS-assisted MgO materials happened to exhibit the highest CO_2 uptake, which is the reason why we chose SDS as the representative surfactant for further investigation.
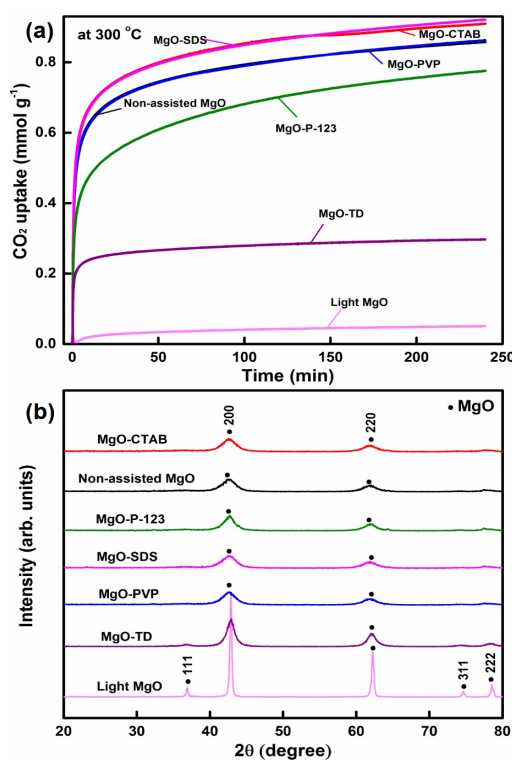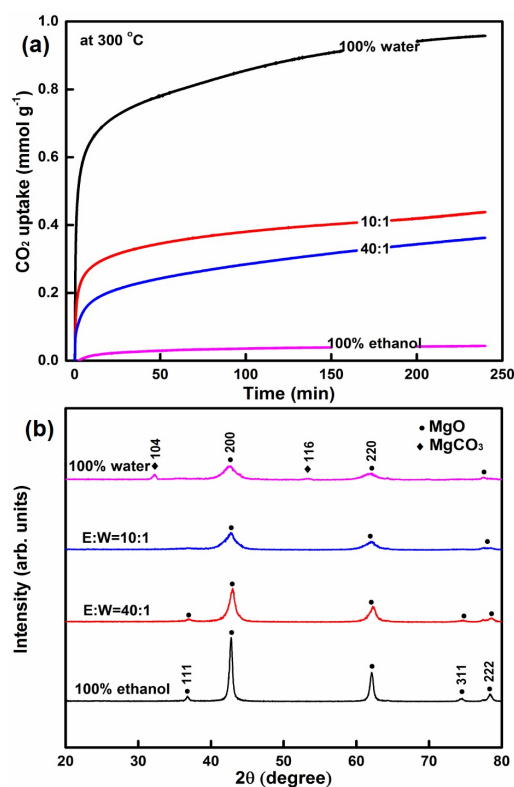

Figure 1. (**a**) The influence of different types of surfactants on the CO_2 capture capacity; (**b**) XRD spectra of MgO compounds with different types of surfactants.

Table 1. Synthetic conditions, texture parameters and CO_2 adsorption capacities of different types of surfactant-assisted MgO.

Sample	Surfactant	Ethanol/Water Ratio	Hydrothermal Conditions (°C and h)	Calcination Conditions (°C and h)	BET Surface Area ($m^2\,g^{-1}$)	Pore Volume ($cm^3\,g^{-1}$)	Average Pore Size (nm)	Crystalline Size (nm)	CO_2 Uptake ($mmol\,g^{-1}$)
MgO	Surfactant-free	1:1	120 and 12	400 and 5	194.3	0.30	3.05	1.3	0.86
MgO	P-123	1:1	120 and 12	400 and 5	305.7	0.42	2.78	2.1	0.78
MgO	PVP	1:1	120 and 12	400 and 5	302.3	0.36	2.40	2.0	0.86
MgO	CTAB	1:1	120 and 12	400 and 5	341.4	0.49	2.90	3.2	0.91
MgO	SDS	1:1	120 and 12	400 and 5	321.7	0.40	2.51	7.1	0.92
MgO-TD	-	1:1	-	400 and 5	363.4	0.53	2.91	6.0	0.29
Light MgO	-	1:1	-	-	25.1	0.17	13.22	32.4	0.05

2.1.2. The Influence of the Ratio of Ethanol to Water on CO_2 Capture

Apparently, the ethanol to water ratio is one of the key parameters that influences the CO_2 capture performance of MgO samples. Figure 2a shows the CO_2 capture capacity of the synthesized MgO with different ratios at 300 °C. Based upon the data, one can see that the CO_2 uptake increased with the increase in water content. The decline in CO_2 uptake with the addition of ethanol may be attributed to a slow hydrolysis rate and a slightly lower solubility of SDS. The structural changes of MgO particles were also investigated by XRD analyses, as shown in Figure 2b. All diffraction peaks of the samples can be indexed to the MgO (JCPDS 45-0946). Notably, two small characteristic peaks of magnesium carbonate ($MgCO_3$) at $2\theta \approx 32.20°$ and $53.35°$ (JCPDS 08-0479) were observed, indicating a little $MgCO_3$ was incorporated in MgO. When the ethanol content was high, a slower hydrolysis rate and a slightly lower solubility of SDS were favorable for the growth of MgO with a higher crystalline degree. The slight shift to a higher angle might be due to the contraction of the lattice constant when the crystalline degree was high [41,42]. It should be noted that the specific surface area increased steadily from 58.7 to 321.3 $m^2\,g^{-1}$ with the rise in water content, while the average pore size is on a gradual decline from 23.52 to 1.88 nm, which is consistent with the CO_2 uptake data, as shown in Table 2.


Figure 2. (**a**) The influence of ratios of ethanol and water on the CO_2 capture capacity; (**b**) XRD spectra of MgO compounds with different ratios of ethanol and water.

Table 2. Synthetic conditions, texture parameters and CO_2 adsorption capacities of sodium dodecyl sulfate (SDS)-assisted MgO with different ratios of ethanol and water.

Sample	Ethanol/Water Ratio	Hydrothermal Conditions (°C and h)	Calcination Conditions (°C and h)	BET Surface Area ($m^2\ g^{-1}$)	Pore Volume ($cm^3\ g^{-1}$)	Average Pore Size (nm)	Crystalline Size (nm)	CO_2 Uptake ($mmol\ g^{-1}$)
MgO-SDS	100% ethanol	120 and 12	400 and 5	58.7	0.69	23.52	18.6	0.04
MgO-SDS	40:1	120 and 12	400 and 5	185.8	0.81	8.67	5.3	0.36
MgO-SDS	10:1	120 and 12	400 and 5	272.4	0.64	4.73	2.8	0.44
MgO-SDS	100% water	120 and 12	400 and 5	321.3	0.30	1.88	5.4	0.96

2.1.3. The Influence of the SDS Amount on CO_2 Capture

To study the effect of the SDS content on CO_2 adsorption, SDS-assisted MgO nanomaterials were prepared with different dosages of SDS as 0.08, 0.1, 0.5, and 1 g, respectively. As shown in Figure 3a, the synthesized MgO compounds with different SDS contents showed a steady increase in CO_2 capture capacity from 0.85 to 0.96 mmol g^{-1}. Table 3 clearly reflects that all the samples exhibited a high specific surface area of more than 321.3 $m^2\ g^{-1}$ and a relatively small average pore size of less than 1.88 nm. The crystal phase of MgO particles was further confirmed by X-ray diffraction. Therefore, the results suggest that the SDS amount has merely little effect on the CO_2 capture capacity.
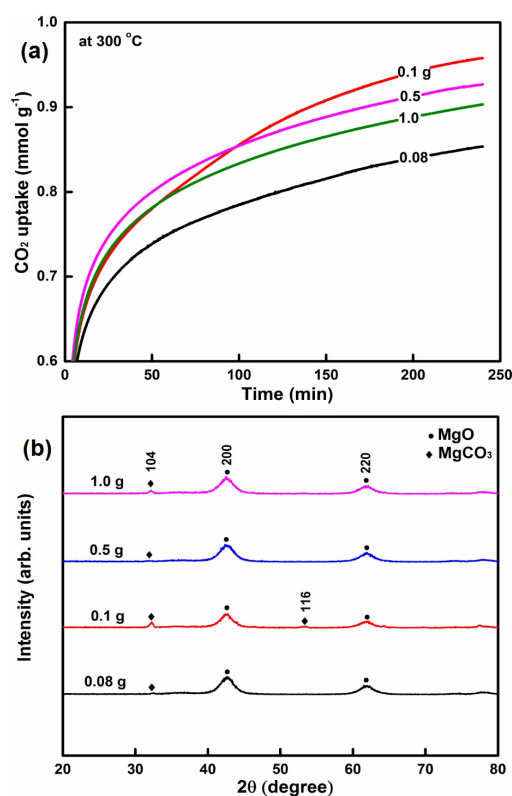
Figure 3. (**a**) The influence of SDS amount on the CO_2 capture capacity; (**b**) XRD spectra of MgO compounds with different amounts of SDS.

Table 3. Synthetic conditions, texture parameters and CO_2 adsorption capacities of SDS-assisted MgO with different loadings.

Sample	Ethanol/Water Ratio	Loading (g)	Hydrothermal Conditions (°C and h)	Calcination Conditions (°C and h)	BET Surface Area ($m^2\ g^{-1}$)	Pore Volume ($cm^3\ g^{-1}$)	Average Pore Size (nm)	Crystalline Size (nm)	CO_2 Uptake ($mmol\ g^{-1}$)
MgO-SDS	100% water	0.08	120 and 12	400 and 5	348.3	0.36	2.04	4.9	0.85
MgO-SDS	100% water	0.1	120 and 12	400 and 5	321.3	0.30	1.88	5.4	0.96
MgO-SDS	100% water	0.5	120 and 12	400 and 5	501.3	0.64	2.55	2.1	0.93
MgO-SDS	100% water	1.0	120 and 12	400 and 5	413.4	0.39	2.31	10.0	0.90

2.1.4. The Influence of Reaction Time on CO_2 Capture

The effect of reaction time was then investigated based on the sample with 0.1 g SDS. As shown in Figure 4a, with prolonging the reaction time, the CO_2 capacity steadily increased from 0.94 to 0.96 mmol g^{-1} between six and 12 h and subsequently there was a noticeable decline from 0.96 to 0.55 mmol g^{-1} between 12 to 72 h. Figure 4b shows the XRD patterns of the synthesized samples. When the reaction time was no longer than 18 h, all samples formed mainly MgO (JCPDS 45-0946) with some $MgCO_3$ (JCPDS 08-0479) impurity observed. With a further prolonging of the reaction time, the $MgCO_3$ content steadily increased. Particularly for the 72 h sample, the majority phase became $MgCO_3$ and the sharp and intense peaks indicated their highly crystalline nature. The major determinant lies in the degree of the urea hydrolysis process. With longer reaction time, the formation of $MgCO_3$ was preferred, which led to a decreased CO_2 capture capacity. Table 4 demonstrates clearly that all the samples possess high specific surface area in the range of 204.0 to 375.2 m^2 g^{-1}, and small average pore size of 1.82 to 2.19 nm.
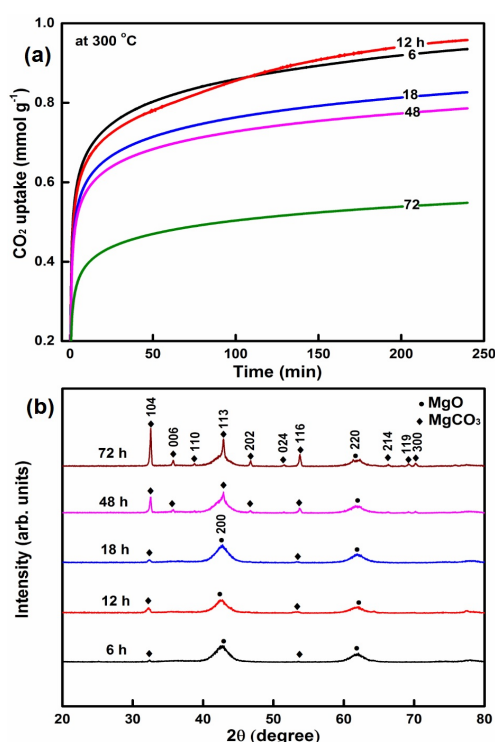
Figure 4. (**a**) The influence of reaction time on the CO_2 capture capacity; (**b**) XRD spectra of MgO compounds at different reaction times.
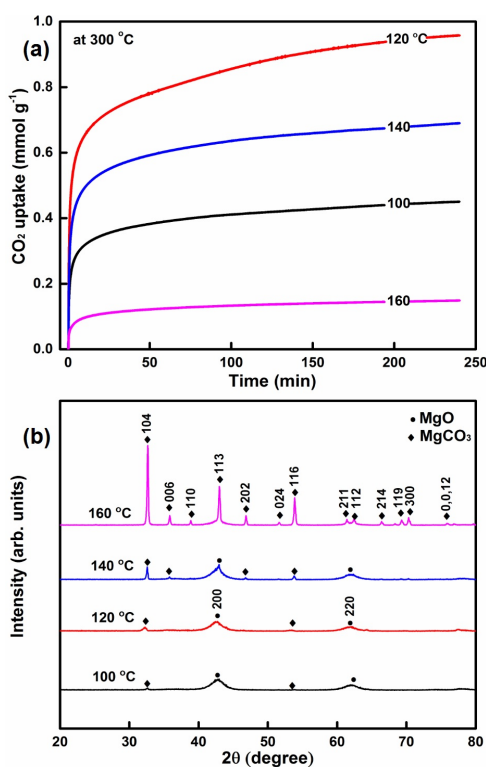
Table 4. Synthetic conditions, texture parameters and CO_2 adsorption capacities of SDS-assisted MgO with different reaction times.

Sample	Ethanol/Water Ratio	Loading (g)	Hydrothermal Conditions (°C and h)	Calcination Conditions (°C and h)	BET Surface Area (m^2 g^{-1})	Pore Volume (cm^3 g^{-1})	Average Pore Size (nm)	Crystalline Size (nm)	CO_2 Uptake (mmol g^{-1})
MgO-SDS	100% water	0.1	120 and 6	400 and 5	369.1	0.35	1.90	11.6	0.94
MgO-SDS	100% water	0.1	120 and 12	400 and 5	321.3	0.30	1.88	5.4	0.96
MgO-SDS	100% water	0.1	120 and 18	400 and 5	276.6	0.40	2.19	20.3	0.83
MgO-SDS	100% water	0.1	120 and 48	400 and 5	204.0	0.19	1.86	55.0	0.79
MgO-SDS	100% water	0.1	120 and 72	400 and 5	375.3	0.34	1.82	43.3	0.55

2.1.5. The Influence of the Reaction Temperature on CO_2 Capture

It is fairly clear that the formation of intermediates is largely affected by the reaction temperatures. Therefore, SDS-assisted MgO particles have been methodically prepared under different temperatures

at 100, 120, 140, and 160 °C, respectively, to further explore the influence of the reaction temperature. Figure 5a shows that the CO_2 uptake went up from 0.45 to 0.96 mmol g^{-1} as the temperature increased from 100 to 120 °C and then declined from 0.96 to 0.15 mmol g^{-1} from 120 to 160 °C. To better understand the circumstances, we also explored the structural changes of all samples synthesized in the temperature range of 100-160 °C by XRD analyses. With the reaction temperature lower than 140 °C, all samples formed mainly MgO (JCPDS 45-0946) with some $MgCO_3$ (JCPDS 08-0479) impurity observed. As the diffraction peaks of $MgCO_3$ became stronger with elevated temperatures, the $MgCO_3$ content steadily increased. The 160 °C sample presented the majority phase of $MgCO_3$ with the sharp and intense peaks indicative of their highly crystalline nature. It is observed that MgO is the main components of the samples synthesized at low temperatures. It is interesting that specific surface area had good correlation with the CO_2 capture capacity (Table 5). For the 100 °C sample, the slow hydrolysis rate at lower temperatures is favorable to form large particles. The higher crystallinity gave rise to a decline in specific surface area, which shows good consistent with the CO_2 capture capacity. The samples fabricated at elevated temperatures are mainly $MgCO_3$. The specific surface area is rather low due to the high decomposition temperature, which coincides well with the CO_2 capture capacity.


Figure 5. (**a**) The influence of reaction temperature on the CO_2 capture capacity; (**b**) XRD spectra of MgO compounds at different reaction temperatures.

Table 5. Synthetic conditions, texture parameters, and CO_2 adsorption capacities of SDS-assisted MgO with different reaction temperatures.

| Sample	Ethanol/Water Ratio	Loading (g)	Hydrothermal Conditions (°C and h)	Calcination Conditions (°C and h)	BET Surface Area (m^2 g^{-1})	Pore Volume (cm^3 g^{-1})	Average Pore Size (nm)	Crystalline Size (nm)	CO_2 Uptake (mmol g^{-1})
MgO-SDS	100% water	0.1	100 and 12	400 and 5	106.8	0.50	9.44	63.4	0.45
MgO-SDS	100% water	0.1	120 and 12	400 and 5	321.3	0.30	1.88	5.4	0.96
MgO-SDS	100% water	0.1	140 and 12	400 and 5	181.7	0.22	2.40	50.1	0.69
MgO-SDS	100% water	0.1	160 and 12	400 and 5	41.1	0.07	3.49	50.7	0.15

2.2. Characterization of SDS-Assisted MgO

　　To clarify the details of the SDS-assisted MgO, XRD, BET, FTIR and SEM analyses were utilized to characterize the MgO sample synthesized with 0.1 g SDS at 120 °C for 12 h. XRD patterns (Figure 5b) showed that the synthesized SDS-assisted samples consisted of a large portion of MgO along with a smaller part of $MgCO_3$. It is noteworthy that urea will hydrolyze within the aqueous magnesium nitrate solution to form different precursors under different operating conditions. The specific surface area of the SDS-assisted MgO was calculated using the Brunauer-Emmett-Teller (BET) method and the pore volume distribution was calculated by the Barrett-Joyner-Halenda (BJH) method. Figure 6a illustrates the N_2 adsorption isotherms of the SDS-assisted samples. The isotherms were classified as type IV with a sharp H3 hysteresis loop, which reveals the existence of slit-type interparticle mesopores in the as-synthesized samples. This type of hysteresis loop is usually spotted on solids comprised of aggregates or agglomerates of particles forming slit shaped pores with a non-uniform size and/or shape [43]. The SDS-assisted MgO sample possesses a high specific surface area of 321.3 m^2 g^{-1}, a high pore volume of 0.30 cm^3 g^{-1}, and a narrow micropore size distribution, with the majority centered at 1.88 nm (Figure 6b). It is obvious that the template SDS contributes tremendously to the fabrication of the porous structure in leaf-like MgO.
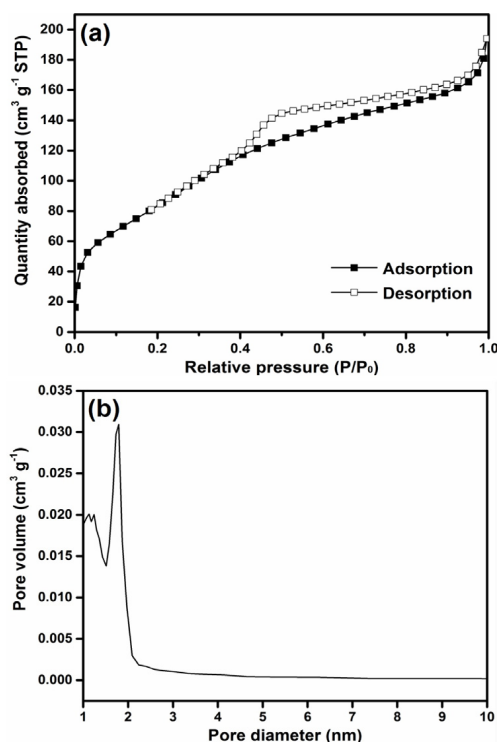

Figure 6. (**a**) Nitrogen adsorption-desorption isotherms and (**b**) pore size distributions of SDS-assisted MgO samples generated hydrothermally and calcined at 400 °C for 5 h.

　　The morphological changes of SDS-assisted MgO materials during the thermal treatment were also examined using SEM analyses. Figure 7a,b indicates that a well-organized lamellate structure of the precursors crystallites is noticeable. The disordered thin-layer morphology of SDS-assisted MgO nanosheet is highly likely correlated with the considerable disorganization caused by the removal of interlayer water molecules after the calcination process, as shown in Figure 7c,d. Besides, well-developed hexagonal prisms crystallites of MgO-TD (Figure 7e,f) are observed, which provides a good explanation in the great variations of CO_2 uptake between the SDS-assisted MgO nanosheet and the MgO-TD due to the significant differences in their morphology.
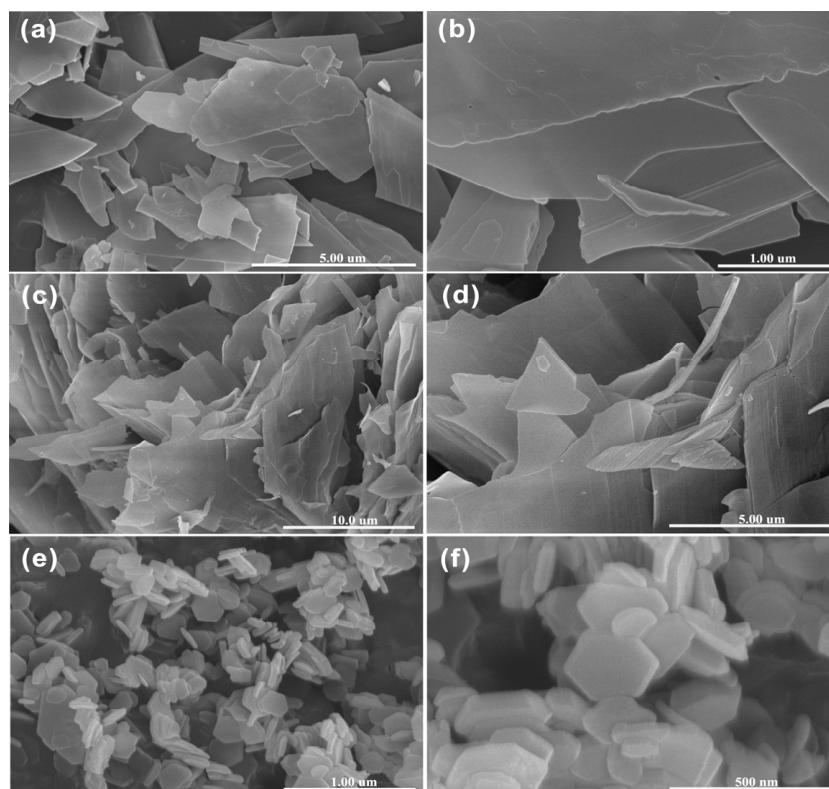
Figure 7. SEM images of (**a**,**b**) precursors; (**c**,**d**) MgO nanosheets after calcination at 400 °C for 5 h; (**e**,**f**) MgO-TC of different magnifications, respectively.

Based on SEM analyses, the possible mechanism is proposed to explain the formation of the SDS-assisted MgO nanosheet in Scheme 1. The surfactants are usually utilized to prepare metal oxide nanoparticles, in which the polar groups directly interact with the particles surface and strongly influence their shape [44]. SDS is an anionic surfactant which can be adsorbed on the surface of precursors and can act as a directing agent by the interaction of negatively charged head groups with the magnesium ion. During the calcination of precursors, the surfactant molecules decomposed and induced the formation of small MgO nanocrystals with plenty of mesopores. The morphology was well preserved in the MgO nanomaterials during the thermal treatment as indicated in Figure 7c,d. Amines are well-recognized for their capacity to bind carbon dioxide. As urea was used in the synthesis of SDS-assisted MgO nano-materials, a representative vibrational FTIR spectrum of the MgO nano-materials was presented in Figure 8d to deny the presence of surface urea/amine species. The adsorption band at 1456 cm^{-1} corresponds to the asymmetric stretch of carbonate ions. The peaks at 1647 and 1087 cm^{-1} were assigned to the asymmetric and symmetric stretch of bidentate carbonates, respectively. The three distinct FTIR bands in the SDS-assisted MgO were chemisorbed on the surface of MgO. The characteristic peak of the OH group at 3398 cm^{-1} was observed as well. The existence of these weak peaks for various carbonate species may be resulted from the adsorption of the atmospheric CO_2 on the surface of MgO [45,46]. Moreover, as there was no sign of the NH stretching vibration from 3150 to 3450 cm^{-1} [47,48], the absence of surface urea/amine species was clearly verified. Besides, no residual surfactants were detected.
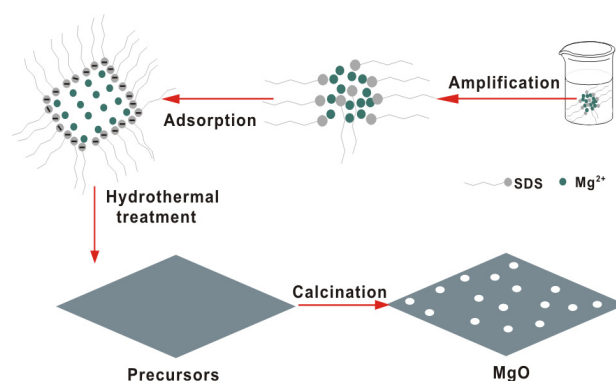
Scheme 1. Schematic illustration of the formation mechanism of SDS-assisted MgO nanosheets.
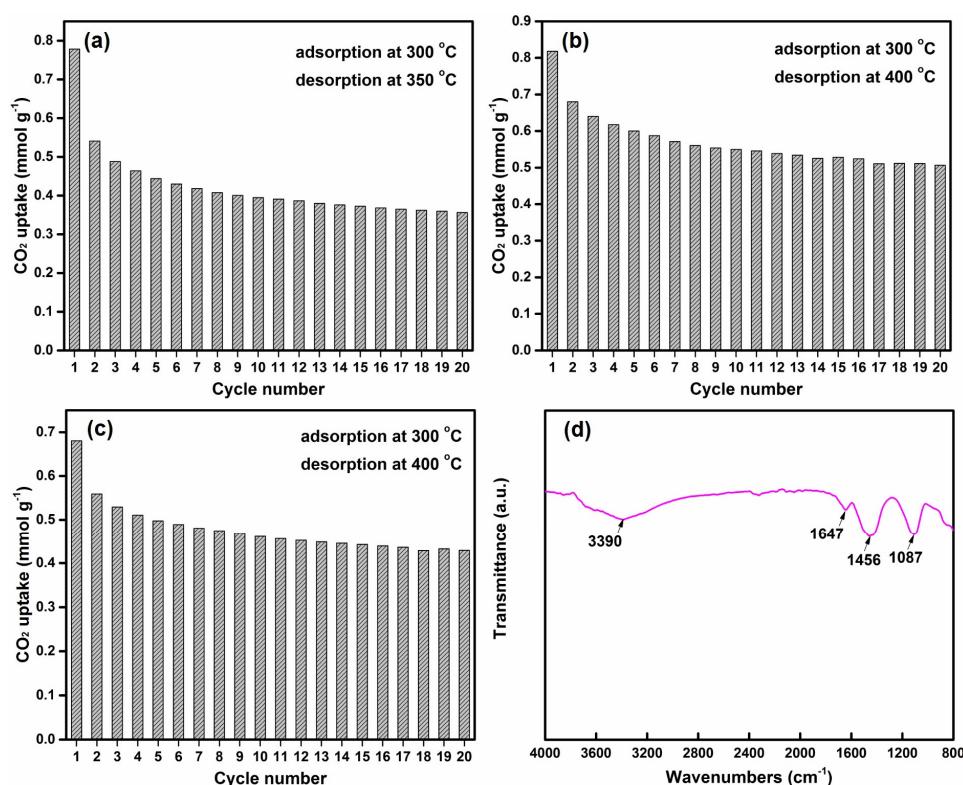
Figure 8. CO_2 uptake over repeated cycles by SDS-assisted MgO particles of (**a**) CO_2 adsorption in 100% CO_2 for 30 min at 300 °C and desorption in 100% N_2 for 30 min at 350 °C; (**b**) CO_2 adsorption in 100% CO_2 for 30 min at 300 °C and desorption in 100% N_2 for 30 min at 400 °C; (**c**) CO_2 adsorption in 50% CO_2 and 50% N_2 for 30 min at 300 °C and desorption in 100% N_2 for 30 min at 400 °C; (**d**) FTIR spectra of SDS-assisted MgO nanomaterial.

2.3. Cycling Stability Tests

High regenerability under repeated cycles of CO_2 adsorption and desorption is an obligatory requirement for CO_2 adsorbents practically utilized in CSU systems. Therefore, the CO_2 adsorption/desorption cycling stability of the synthetic SDS-assisted MgO was comprehensively examined via typical TSA procedures with circulation times fixed at 20 cycles. Figure 8a,b show the continuous adsorption/desorption cycling stability of the synthetic SDS-assisted MgO performed at different desorption temperatures (350 or 400 °C). During the first few cycles, the CO_2 capture capacity of SDS-assisted MgO particles degraded slightly, and in later cycles the uptake displays an excellent regenerability in terms of both rate and extent of uptake of CO_2. Notably, the comparatively

obvious decline in CO_2 uptake initially occurred at 350 °C may be attributed to the incomplete decomposition of $MgCO_3$ due to the unsuitable desorption temperature. It is noteworthy that although the CO_2 uptake of SDS-assisted MgO nanoparticles has met a gradual decline of 0.1 mmol g^{-1} when exposed to 50% CO_2 atmosphere during the adsorption period, as shown in Figure 8c, the adsorption capacity became considerably stable with a reversible capacity of more than 0.4 mmol g^{-1}. In general, it can be concluded that the CO_2 adsorption performance became weakened to a certain extent with the decrease in CO_2 concentration. Figure 8b indicated that the CO_2 capture capacity of the SDS-assisted MgO sample eventually reaches a steady value of 0.5 mmol g^{-1} without further significant degradation, suggesting a great prospect of application in the sorption-enhanced hydrogen production processes [49,50].

Additionally, we have explored the main reason for the capacity decay during several cycles using both BET and SEM techniques. After adsorption/desorption process for 20 times, the disordered thin-layer morphology of the SDS-assisted MgO nanosheet (Figure 9a) was totally destroyed into pieces and a high desorption temperature required promoted agglomeration of leaf-like particles into a block mass (Figure 9b). Besides, BET analysis showed that after 4 cycles, the specific surface area of SDS-assisted MgO nanomaterial showed a downtrend from 321.3 to 260 m^2 g^{-1}, which shows good consistency with the observed SEM images. The results demonstrated that the main reason for the capacity decay observed in the sorbents over repeated cycles was the aggregation due to the grievous desorption condition leading to an irreversible decline in active sites on the surface and severe damage to the specific morphology.
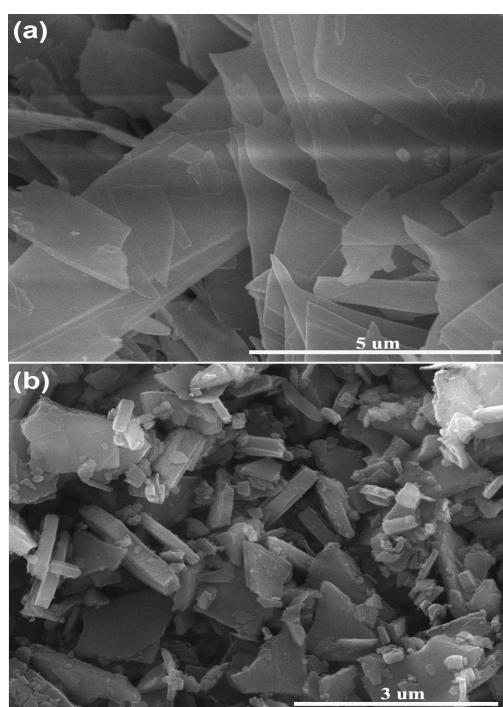

Figure 9. SEM images of (**a**,**b**) SDS-assisted MgO nanoparticles after adsorption/desorption for 20 cycles.

3. Materials and Methods

3.1. Materials

Magnesium nitrate hexahydrate ($Mg(NO_3)_2 \cdot 6H_2O$, 99%), urea ($CO(NH_2)_2$, 99%), and sodium dodecyl sulfate (SDS) were purchased from Sinopharm Chemical Reagent Co Ltd (Shanghai, China). All chemicals were used as received without further purification. Deionized water was utilized in all the experimental processes.

3.2. Sample Preparation

Samples of SDS-assisted porous MgO were prepared by urea hydrolysis assisted precipitation of magnesium hydroxide from magnesium nitrate aqueous solution followed by thermal decomposition of the precipitated magnesium hydroxide. Typically, 3 g of urea (0.05 mol $CO(NH_2)_2$) and appropriate amounts of magnesium nitrate hexahydrate (2.56 g of $Mg(NO_3)_2 \cdot 6H_2O$ for maintaining urea:Mg mole ratio of 5) were mixed in 50 mL of water with the addition of certain amounts of sodium dodecyl sulfate (0.1 g SDS) and stirred vigorously in a Teflon lined stainless steel autoclave at room temperature. The autoclave was then treated hydrothermally in a preheated oven at 120 °C for 12 h. The resulting precipitates were separated by filtration and repeatedly washed with DI water several times and dried at 70 °C overnight in the oven. Dried powders were next ground in a crucible, and calcined at 400 °C for 5 h in air. In all cases, the temperature of the furnace was increased at a very slow rate of 1 °C min^{-1} until the desired temperatures were attained.

3.3. Sample Characterization

Phase compositions and crystallographic structures of the samples were examined by X-ray diffractometry (XRD: Shimadzu XRD-7000 diffractometer, power 40 KV, 30 mA) using Cu Kα radiation in the 2θ range from 5° to 80° with a scanning rate of 5° min^{-1}. As there is no diffraction peak observed in the range from 5° to 80°, we only presented the XRD patterns in the range of 20° to 80° to make them clearer. Size and morphology of the sample grains were measured via scanning electron microscopy (SEM, S-4800). The Brunauer-Emmett-Teller (BET, Builder SSA-7000) method was utilized to calculate the specific surface area of the prepared samples using the adsorption branch acquired at a relative pressure (P/P_0) range of 0.05–0.30. Molecular speciation of the samples was explored by Fourier transform infrared spectroscopy (FTIR: Bruker Vertex 70 spectrophotometer).

3.4. Evaluation of CO_2 Adsorption Capacity

CO_2 uptake by the samples was determined from variations in sample weight under a flow of 100% dry CO_2 at atmospheric pressure as measured with a thermogravimetric analyzer (TGA, Q50 TA Instrument). The flow rates of N_2 and CO_2 were controlled by a mass flow controller (MFC). All samples were pre-calcined at 450 °C for 1 h under a flow of 100% high purity nitrogen (20 mL min^{-1}) giving consideration to remove the preabsorbed species (atmospheric CO_2, water, etc.). The measurements started by switching the gas from nitrogen to CO_2 with a constant flow of high purity CO_2 (1 atm, 40 mL min^{-1}) at 300 °C for 4 h. With regard for the regenerability of the samples under repeated cycles, CO_2 adsorption was performed at 300 °C in the flow of 100% CO_2 for 30 min and desorption was performed at 350 °C or 400 °C in the flow of 100% nitrogen for 30 min. The cycles of adsorption and desorption were repeated 20 times

4. Conclusions

This work sheds light on the synthesis and utilization of an original SDS-assisted MgO-based porous adsorbent for CO_2 capture at intermediate temperatures. The mesoporous MgO adsorbents are successfully synthesized by a simple urea hydrolysis method from aqueous magnesium nitrate solution with a fully disordered layer structure. With the assistance provided by the surfactant SDS the fabricated materials exhibited a uniform ordered narrow mesopores distribution. Comparison of CO_2 capture performances indicated that with the same surfactant SDS, the SDS content had little effect on CO_2 capture capacity. The effect of ethanol to water ratios, reaction time, and reaction temperature have been thoroughly investigated. The highest performance was found to dissolve SDS in pure DI water. The superlative reaction temperature was 120 °C and at least 12 h was needed for the urea hydrolysis process to be completed comprehensively. The XRD patterns provided a clearer understanding of the reaction mechanism. Typically, the SDS-assisted MgO materials possessed the highest CO_2 capture capacity of 0.96 mmol g^{-1} with a high specific surface area of 321.3 m^2 g^{-1}

at moderate temperatures (~300 °C). We suspect that the high CO_2 capture capacity should be related to both the high specific surface area and high surface defects or active adsorption sties, etc. The regenerability of the newly fabricated nanomaterials has been further investigated using a TSA process, which demonstrated a pretty excellent reversible CO_2 uptake of more than 0.5 mmol g^{-1} through multi cycles. The mesoporous MgO materials which possess awesome reactivity and stability in multi cycle processes show significant potential to halt the increasing global CO_2 emissions.

Author Contributions: Q.W. conceived and designed the experiments; W.G. performed the experiments and analyzed the data; T.Z. and B.L. contributed reagents/materials/analysis tools; W.G. and Q.W. wrote the paper.

Conflicts of Interest: The authors declare no conflict of interest.

References

1. Markewitz, P.; Kuckshinrichs, W.; Leitner, W.; Linssen, J.; Zapp, P.; Bongartz, R.; Schreiber, A.; Müller, T.E. Worldwide innovations in the development of carbon capture technologies and the utilization of CO_2. *Energy Environ. Sci.* **2012**, *5*, 7281–7305. [CrossRef]
2. Mikkelsen, M.; Jørgensen, M.; Krebs, F.C. The teraton challenge. A review of fixation and transformation of carbon dioxide. *Energy Environ. Sci.* **2010**, *3*, 43–81. [CrossRef]
3. Schrag, D.P. Preparing to capture CO_2. *Science* **2007**, *315*, 812–813. [CrossRef] [PubMed]
4. Wang, J.; Huang, L.; Yang, R.; Zhang, Z.; Wu, J.; Gao, Y.; Wang, Q.; O'Hare, D.; Zhong, Z. Recent advances in solid sorbents for CO_2 capture and new development trends. *Energy Environ. Sci.* **2014**, *7*, 3478–3518. [CrossRef]
5. Wang, Q.; Luo, J.; Zhong, Z.; Borgna, A. CO_2 capture by solid adsorbents and their applications: Current status and new trends. *Energy Environ. Sci.* **2011**, *4*, 42–55. [CrossRef]
6. Samanta, A.; Zhao, A.; Shimizu, G.K.H.; Sarkar, P.; Gupta, R. Post-combustion CO_2 capture using solid sorbents: A review. *Ind. Eng. Chem. Res.* **2012**, *51*, 1438–1463. [CrossRef]
7. Zhang, K.; Li, X.S.; Duan, Y.; King, D.L.; Singh, P.; Li, L. Roles of double salt formation and $NaNO_3$ in Na_2CO_3-promoted MgO absorbent for intermediate temperature CO_2 removal. *Int. J. Greenh. Gas Control* **2013**, *12*, 351–358. [CrossRef]
8. Chakradhar, A.; Burghaus, U. Carbon dioxide adsorption on MgO(001)—CO_2 kinetics and dynamics. *Surf. Sci.* **2013**, *616*, 171–177. [CrossRef]
9. Plaza, M.G.; Pevida, C.; Arias, B.; Casal, M.D.; Martín, C.F.; Fermoso, J.; Rubiera, F.; Pis, J.J. Different approaches for the development of low-cost CO_2 adsorbents. *J. Environ. Eng.* **2009**, *135*, 426–432. [CrossRef]
10. Harada, T.; Simeon, F.; Hamad, E.Z.; Hatton, T.A. Alkali metal nitrate-promoted high-capacity MgO adsorbents for regenerable CO_2 capture at moderate temperatures. *Chem. Mater.* **2015**, *27*, 1943–1949. [CrossRef]
11. Goff, G.S.; Rochelle, G.T. Monoethanolamine degradation: O_2 mass transfer effects under CO_2 capture conditions. *Ind. Eng. Chem. Res.* **2004**, *43*, 6400–6408. [CrossRef]
12. Vu, A.-T.; Park, Y.; Jeon, P.R.; Lee, C.-H. Mesoporous MgO sorbent promoted with KNO_3 for CO_2 capture at intermediate temperatures. *Chem. Eng. J.* **2014**, *258*, 254–264. [CrossRef]
13. Vu, A.-T.; Ho, K.; Jin, S.; Lee, C.-H. Double sodium salt-promoted mesoporous MgO sorbent with high CO_2 sorption capacity at intermediate temperatures under dry and wet conditions. *Chem. Eng. J.* **2016**, *291*, 161–173. [CrossRef]
14. Lepaumier, H.; Martin, S.; Picq, D.; Delfort, B.; Carrette, P.-L. New amines for CO_2 capture. III. effect of alkyl chain length between amine functions on polyamines degradation. *Ind. Eng. Chem. Res.* **2010**, *49*, 4553–4560. [CrossRef]
15. Knuutila, H.; Svendsen, H.; Anttila, M. CO_2 capture from coal-fired power plants based on sodium carbonate slurry; a systems feasibility and sensitivity study. *Int. J. Greenh. Gas Control* **2009**, *3*, 143–151. [CrossRef]

16. Gao, Y.; Zhang, Z.; Wu, J.; Yi, X.; Zheng, A.; Umar, A.; O'Hare, D.; Wang, Q. Comprehensive investigation of CO_2 adsorption on Mg-Al-CO_3 LDH-derived mixed metal oxides. *J. Mater. Chem. A* **2013**, *1*, 12782–12790. [CrossRef]

17. Choi, S.; Drese, J.H.; Jones, C.W. Adsorbent materials for carbon dioxide capture from large anthropogenic point sources. *ChemSusChem* **2009**, *2*, 796–854. [CrossRef] [PubMed]

18. Yong, Z.; Rodrigues, A.E. Adsorption of carbon dioxide at high temperature—A review. *Sep. Purif. Technol.* **2002**, *26*, 195–205. [CrossRef]

19. Yong, Z.; Mata, V.; Rodrigues, A.E. Adsorption of carbon dioxide onto hydrotalcite-like compounds (HTlcs) at high temperatures. *Ind. Eng. Chem. Res.* **2001**, *40*, 204–209. [CrossRef]

20. Lee, J.M.; Min, Y.J.; Lee, K.B.; Jeon, S.G.; Na, J.G.; Ryu, H.J. Enhancement of CO_2 sorption uptake on hydrotalcite by impregnation with K_2CO_3. *Langmuir* **2010**, *26*, 18788–18797. [CrossRef] [PubMed]

21. Ding, Y.; Alpay, E. Equilibria and kinetics of CO_2 adsorption on hydrotalcite adsorbent. *Chem. Eng. Sci.* **2000**, *55*, 3461–3474. [CrossRef]

22. Bian, S.-W.; Baltrusaitis, J.; Galhotra, P.; Grassian, V.H. A template-free, thermal decomposition method to synthesize mesoporous MgO with a nanocrystalline framework and its application in carbon dioxide adsorption. *J. Mater. Chem.* **2010**, *20*, 8705–8710. [CrossRef]

23. Hanif, A.; Dasgupta, S.; Nanoti, A. Facile synthesis of high surface area mesoporous MgO with excellent high temperature CO_2 adsorption potential. *Ind. Eng. Chem. Res.* **2016**, *55*, 8070–8078. [CrossRef]

24. Zhao, Z.; Dai, H.; Du, Y.; Deng, J.; Zhang, L.; Shi, F. Solvo- or hydrothermal fabrication and excellent carbon dioxide adsorption behaviors of magnesium oxides with multiple morphologies and porous structures. *Mater. Chem. Phys.* **2011**, *128*, 348–356. [CrossRef]

25. Han, K.K.; Zhou, Y.; Lin, W.G.; Zhu, J.H. One-pot synthesis of foam-like magnesia and its performance in CO_2 adsorption. *Microporous Mesoporous Mater.* **2013**, *169*, 112–119. [CrossRef]

26. Seo, Y.; Jo, S.H.; Ryu, C.K.; Yi, C.K. Effects of water vapor pretreatment time and reaction temperature on CO_2 capture characteristics of a sodium-based solid sorbent in a bubbling fluidized-bed reactor. *Chemosphere* **2007**, *69*, 712–718. [CrossRef] [PubMed]

27. Yang, X.; Zhao, L.; Xiao, Y. Affecting mechanism of activation conditions on the performance of $NaNO_3$-modified dolomite for CO_2 capture. *Asia-Pac. J. Chem. Eng.* **2015**, *10*, 754–763. [CrossRef]

28. Harada, T.; Hatton, T.A. Colloidal nanoclusters of MgO coated with alkali metal nitrates/nitrites for rapid high capacity CO_2 capture at moderate temperature. *Chem. Mater.* **2015**, *27*, 8153–8161. [CrossRef]

29. Hanif, A.; Dasgupta, S.; Nanoti, A. High temperature CO_2 adsorption by mesoporous silica supported magnesium aluminum mixed oxide. *Chem. Eng. J.* **2015**, *280*, 703–710. [CrossRef]

30. Zhang, K.; Li, X.S.; Chen, H.; Singh, P.; King, D.L. Molten salt promoting effect in double salt CO_2 absorbents. *J. Phys. Chem. C* **2016**, *120*, 1089–1096. [CrossRef]

31. Ding, Y.; Alpay, E. High temperature recovery of CO_2 from flue gases using hydrotalcite adsorbent. *Process Saf. Environ. Prot.* **2001**, *79*, 45–51. [CrossRef]

32. Ram Reddy, M.K.; Xu, Z.P.; Lu, G.Q.; Diniz da Costa, J.C. Layered double hydroxides for CO_2 capture: Structure evolution and regeneration. *Ind. Eng. Chem. Res.* **2006**, *45*, 7504–7509. [CrossRef]

33. Yavuz, C.T.; Shinall, B.D.; Iretskii, A.V.; White, M.G.; Golden, T.; Atilhan, M.; Ford, P.C.; Stucky, G.D. Markedly improved CO_2 capture efficiency and stability of gallium substituted hydrotalcites at elevated temperatures. *Chem. Mater.* **2009**, *21*, 3473–3475. [CrossRef]

34. Mondal, M.K.; Balsora, H.K.; Varshney, P. Progress and trends in CO_2 capture/separation technologies: A review. *Energy* **2012**, *46*, 431–441. [CrossRef]

35. Song, G.; Zhu, X.; Chen, R.; Liao, Q.; Ding, Y.-D.; Chen, L. An investigation of CO_2 adsorption kinetics on porous magnesium oxide. *Chem. Eng. J.* **2016**, *283*, 175–183. [CrossRef]

36. Han, K.K.; Zhou, Y.; Chun, Y.; Zhu, J.H. Efficient MgO-based mesoporous CO_2 trapper and its performance at high temperature. *J. Hazard. Mater.* **2012**, *203*, 341–347. [CrossRef] [PubMed]

37. Siriwardane, R.V.; Robert, W.; Stevens, J. Novel regenerable magnesium hydroxidesorbents for CO_2 capture at warm gas temperatures. *Ind. Eng. Chem. Res.* **2009**, *48*, 2135–2141. [CrossRef]

38. Choi, D.-H.; Lee, J.B.; Eom, T.H.; Baek, J.I.; Jegarl, S.; Ryu, C.K. Study of MgO-based dry regenerable sorbent for sorption enhanced water gas shift reaction. *Renew. Energy* **2013**, *54*, 144–149. [CrossRef]

39. Henrist, C.; Mathieu, J.P.; Vogels, C.; Rulmont, A.; Cloots, R.J. Morphological study of magnesium hydroxide nanoparticles precipitated in dilute aqueous solution. *J. Cryst. Growth* **2003**, *249*, 321–330. [CrossRef]

40. Ruminski, A.M.; Jeon, K.-J.; Urban, J.J. Size-dependent CO_2 capture in chemically synthesized magnesium oxide nanocrystals. *J. Mater. Chem.* **2011**, *21*, 11486–11491. [CrossRef]

41. Ding, Y.; Zhang, G.; Wu, H.; Hai, B.; Wang, L.; Qian, Y. Nanoscale magnesium hydroxide and magnesium oxide powders: Control over size, shape, and structure via hydrothermal synthesis. *Chem. Mater.* **2001**, *13*, 435–440. [CrossRef]

42. Zhang, T.; Zhu, H.; Croue, J.P. Production of sulfate radical from peroxymonosulfate induced by a magnetically separable $CuFe_2O_4$ spinel in water: Efficiency, stability, and mechanism. *Environ. Sci. Technol.* **2013**, *47*, 2784–2791. [CrossRef] [PubMed]

43. Kruk, M.; Jaroniec, M. Gas adsorption characterization of ordered organic-inorganic nanocomposite materials. *Chem. Mater.* **2001**, *13*, 3169–3183. [CrossRef]

44. Dhaouadi, H.; Chaabane, H.; Touati, F. $Mg(OH)_2$ nanorods synthesized by a facile hydrothermal method in the presence of CTAB. *Nano-Micro Lett.* **2011**, *3*, 153–159. [CrossRef]

45. Qiao, Y.; Wang, J.; Zhang, Y.; Gao, W.; Harada, T.; Huang, L.; Hatton, T.A.; Wang, Q. Alkali nitrates molten salt modified commercial MgO for intermediate-temperature CO_2 capture: Optimization of the Li/Na/K ratio. *Ind. Eng. Chem. Res.* **2017**, *56*, 1509–1517. [CrossRef]

46. Sutradhar, N.; Sinhamahapatra, A.; Pahari, S.K.; Pal, P.; Bajaj, H.C.; Mukhopadhyay, I.; Panda, A.B. Controlled synthesis of different morphologies of MgO and their use as solid base catalysts. *J. Phys. Chem. C* **2011**, *115*, 12308–12316. [CrossRef]

47. Faria, M.; de Pinho, M.N. Phase segregation and gas permeation properties of poly(urethane urea) bi-soft segment membranes. *Eur. Polym. J.* **2016**, *82*, 260–276. [CrossRef]

48. Ren, L.-F.; Geng, J.; Chen, T.; Guo, P.-Y.; Qiang, T.-T. Synthesis and application of hyperbranched poly(urethane-urea) finishing agent with amino groups. *J. Appl. Polym. Sci.* **2016**, *133*. [CrossRef]

49. Abbasi, E.; Hassanzadeh, A.; Abbasian, J. Regenerable MgO-based sorbent for high temperature CO_2 removal from syngas: 2. Two-zone variable diffusivity shrinking core model with expanding product layer. *Fuel* **2013**, *105*, 128–134. [CrossRef]

50. Abbasi, E.; Hassanzadeh, A.; Zarghami, S.; Arastoopour, H.; Abbasian, J. Regenerable MgO-based sorbent for high temperature CO_2 removal from syngas: 3. CO_2 capture and sorbent enhanced water gas shift reaction. *Fuel* **2013**, *137*, 260–268. [CrossRef]